TURBULENCE MODELLING OVER TWO-DIMENSIONAL HILLS USING AN ALGEBRAIC REYNOLDS STRESS EXPRESSION

R. YING and V. M. CANUTO
NASA, Goddard Institute for Space Studies, New York, N.Y., 10025, U.S.A

(Received in final form 4 September, 1995)

Abstract. We carry out model studies of turbulence quantities for flow over two-dimensional hills using a non-hydrostatic version of the Regional Atmospheric Modeling System (RAMS). We test two turbulence closure models: the first one is an explicit Algebraic Reynolds Stress Model (ARSM) and the second one is a combination of the ARSM and a transport equation for the shear stress $\overline{uw}$. Model predictions for the turbulent stresses are compared with data from a wind-tunnel experiment containing isolated two-dimensional hills of varying slope. From the comparison, it is concluded that the first model can only predict the normal stresses adequately while the second model provides satisfactory predictions for the normal stresses as well as giving an improved result for the shear stress $\overline{uw}$.

1. Introduction

The study of the transport and dispersion of pollutants in the atmosphere is usually carried out using turbulent dispersion models, which require the turbulent normal stresses $\overline{u^2}$, $\overline{v^2}$ and $\overline{w^2}$, where u, v, and w are turbulent velocity components along x, y and z directions. The estimate of these quantities, therefore, will significantly affect the performance of the dispersion models. In the past, turbulent normal stresses were often given by oversimplified models. For example, in some cases, turbulence was assumed to be isotropic with the turbulent normal stresses given by $\overline{u^2} = \overline{v^2} = \overline{w^2} = \frac{2}{3}E$, where E is the turbulent kinetic energy. More frequently, turbulent normal stresses were given by empirical expressions containing a number of parameters that had to be adjusted a posteriori from case to case (cf. Hanna, 1968; Panofsky *et al.*, 1977). The main drawback of this type of model is the lack of predictive power.

As far as turbulence modelling is concerned, lower-order turbulence models, including zero-equation models, which do not solve transport equations for turbulent quantities, one-equation models, in which one solves the transport equation for the turbulent kinetic energy E, and two-equation models, in which one solves the transport equations for E and another quantity related to the turbulence length scale (most frequently, the energy dissipation rate ϵ), are all based on the Boussinesq eddy-viscosity assumption. The eddy-viscosity concept assumes that the Reynolds stresses $\overline{u_i u_j}$ are proportional to the mean velocity gradients as

$$\overline{u_i u_j} = -\nu_t \left(\frac{\partial \overline{U_i}}{\partial x_j} + \frac{\partial \overline{U_j}}{\partial x_i} \right) + \frac{2}{3}\delta_{ij} E. \tag{1}$$

Boundary-Layer Meteorology **77:** 69–99, 1996.

where ν_t is the eddy-viscosity.

When applying Equation (1) to a two-dimensional boundary-layer flow uniform in the flow direction, all three normal stresses would be given by $\frac{2}{3}E$. This result contradicts many wind-tunnel measurements (e.g., Hunt and Fernholz, 1975). Specifically, in the EPA wind-tunnel experiment RUSHIL (Khurshudyan *et al.*, 1981), the turbulent normal stresses measured near the surface over flat terrain are given by $\overline{u^2} = 1.05E$, $\overline{v^2} = 0.59E$ and $\overline{w^2} = 0.36E$ (the flow is in the x direction). Clearly, turbulence models based on the eddy-viscosity assumption can not even predict the observed difference between the normal stresses in this very simple case, much less be successful in applications to highly inhomogeneous flows, such as those involved in complex terrain. Therefore, when one needs to make reasonable predictions of the normal stresses, the development of higher-order turbulence models becomes inevitable.

The full second-order closure model employs transport equations for all the components of the Reynolds stress tensor (in general flows, there are six independent components). The task of solving a large number of partial differential equations is by no means trivial and this renders the model rather uneconomical. As a compromise between accuracy and efficiency, several authors (Rodi, 1972; Launder *et al.*, 1975; Pope, 1975; Taulbee, 1992; Gatski and Speziale, 1993) have developed algebraic Reynolds stress models (ARSMs), which do not entail a priori adoption of the eddy-viscosity concept. Rather, these models are derived directly from the transport equations for the Reynolds stresses. In brief, these derivations consist of approximating those terms in the transport equations that contain derivatives of the Reynolds stresses in some fashion so that these equations become algebraic. Among them, of particular interest here is the work of Pope, who has presented an explicit algebraic relation for the Reynolds stresses in two-dimensional turbulent flows.

Although Pope's work went to some extent unnoticed, it contains nice features that drew our attention. Specifically, the formulation seems promising in providing an efficient and adequate tool in the study of the Reynolds stresses in complex terrain. The main purpose of this paper is to explore Pope's work by examining its performance in a wind-tunnel experiment. The specific wind-tunnel experiment we choose is the EPA experiment RUSHIL which provides complete mean and turbulent field data for a neutrally stratified flow over isolated, two-dimensional hills of variable shape.

In the last two decades, the study of flow over hills has received considerable attention, because of its importance in pollutant dispersion predictions and wind energy applications. In a most influential theoretical study of turbulent flow over hills (Jackson and Hunt, 1975) the flow is divided into two layers, an inner layer where the stress perturbation can affect the mean flow and an outer layer where the flow is essentially inviscid. This theory has formed the basis for a series of models developed later (Mason and Sykes, 1979; Britter *et al.*, 1981; Walmsley *et al.*, 1982, 1986; Taylor *et al.*, 1983; Hunt *et al.*, 1988). The key to this approach is a careful

scale analysis of the magnitudes of the various terms in the turbulence equation. It is known that at the bottom of the inner layer, the turbulence is approximately in local equilibrium, where the advection and transport are small, and the production is balanced by dissipation. In the outer layer, because the mean strain rates change rapidly compared to the eddy turnover time, the advection of turbulent energy from upstream becomes important and there is no balance between production and dissipation. In Jackson and Hunt's work, the equation of motion is linearized so that it can only apply to flow over low hills. The analyses in this work, however, have had a profound influence on the way to view flow over hills of steepness greater than the linearized approach strictly accommodates.

On the other hand, the numerical simulation method can solve the non-linear equations of motion with the addition of different turbulence closure schemes, and is not restricted to flow over low hills. Among the many who carried out numerical simulations of flow over complex terrain, Beljaars *et al.* (1987) and Zeman and Jensen (1987) compared their computational results using different turbulence closure models to the Askervein field experimental data (Taylor and Teunissen, 1985). They concluded that only sophisticated closure models, such as the $E - \epsilon - \tau$ or the second-order closure, can correctly predict the stress changes over a hill. Ayotte *et al.* (1994) and Xu *et al.* (1994) compared the impacts of a variety of turbulence closure schemes on flow over complex terrain. Since their computations were based on terrains used neither for wind-tunnel nor field experiments, their results were not directly compared with measured data.

Through literature review, we found that in the past, little attention has been paid to the study of the behavior of normal stresses for flow over complex terrain. Also, the many normal stress data measured in wind-tunnel experiments were rarely used for comparison with simulation results. Our study will concentrate on these two aspects.

In this study, we solve a full set of primitive non-hydrostatic dynamic equations for mean flow quantities using a finite-difference method. The numerical code RAMS (the Regional Atmospheric Modeling System of Colorado State University) will be employed to perform the numerical calculation. The original RAMS code will be supplemented by our new turbulence models. In the first model, Pope's formulation will be used to calculate all the components in the Reynolds stress tensor. In the second model, Pope's formulation will only be used to calculate the normal stresses and a transport equation will be used to solve for the shear stress $\overline{uw}$. In addition, these two models need to be solved in conjunction with the transport equations for the turbulent kinetic energy E and the energy dissipation rate ϵ. To account for complex terrain, we use the terrain-following coordinate system available in RAMS (Clark, 1977), in which an irregular lower boundary is transformed into a plane. We shall make a detailed comparison of the simulation results using the above-mentioned two turbulence models and the wind-tunnel data, and assess Pope's model.

2. Theoretical Formulations

2.1. NON-HYDROSTATIC FLOW MODEL OVER COMPLEX TERRAIN

The mean flow velocity is governed by the following equation of motion

$$\frac{d\overline{U_i}}{dt} + c_p\Theta_0\frac{\partial\pi'}{\partial x_i} = \delta_{i3}g\left(\frac{\overline{\Theta}}{\Theta_0} - 1\right) - \frac{\partial}{\partial x_j}\overline{u_iu_j}, \tag{2}$$

while the pressure is determined by a non-hydrostatic equation

$$\frac{\partial\pi'}{\partial t} + \frac{R\Pi_0}{c_v\rho_0\Theta_0}\frac{\partial}{\partial x_j}(\rho_0\Theta_0\overline{U_j}) = 0. \tag{3}$$

In these equations, $\overline{U_i}$ and $\overline{\Theta}$ are the ensemble averages of the ith velocity component and the potential temperature; ρ_0, Θ_0 and Π_0 are the density, potential temperature and dimensionless pressure of the initial unperturbed state of the atmosphere which is taken to be isentropic and at rest; π' is the deviation of pressure from Π_0; $\overline{u_iu_j}$ are the Reynolds stresses; R is the gas constant for dry air; c_p and c_v are the specific heats at constant pressure and volume respectively and g is the acceleration due to gravity. For detailed derivation and numerical solution procedures of the above equations, the reader is referred to our previous paper (Ying *et al.*, 1994).

In the presence of complex terrain with surface height $z_g(x, y)$ and boundary layer height s, all equations are transformed from Cartesian coordinates (x, y, z) to a terrain following coordinate system (x, y, η) where

$$\eta = s\frac{z - z_g(x, y)}{s - z_g(x, y)}. \tag{4}$$

2.2. POPE'S EXPLICIT ALGEBRAIC REYNOLDS STRESS MODEL (ARSM)

Pope's ARSM is derived from the transport equation for the Reynolds stresses $\overline{u_iu_j}$ modelled by Launder *et al.* (1975), which can be written as

$$\begin{aligned}\frac{d\overline{u_iu_j}}{dt} &= D_f(\overline{u_iu_j}) - \overline{u_iu_k}\frac{\partial\overline{U_j}}{\partial x_k} - \overline{u_ju_k}\frac{\partial\overline{U_i}}{\partial x_k} - \frac{2}{3}\epsilon\delta_{ij} - C_1\frac{\epsilon}{E}\left(\overline{u_iu_j} - \frac{2}{3}\delta_{ij}E\right)\\ &\quad + \frac{C_2 + 8}{11}\left(\overline{u_iu_k}\frac{\partial\overline{U_j}}{\partial x_k} + \overline{u_ju_k}\frac{\partial\overline{U_i}}{\partial x_k} + \frac{2}{3}P\delta_{ij}\right)\\ &\quad - \frac{30C_2 - 2}{55}E\left(\frac{\partial\overline{U_i}}{\partial x_j} + \frac{\partial\overline{U_j}}{\partial x_i}\right) + \frac{8C_2 - 2}{11}\\ &\quad \times\left(\overline{u_iu_k}\frac{\partial\overline{U_k}}{\partial x_j} + \overline{u_ju_k}\frac{\partial\overline{U_k}}{\partial x_i} + \frac{2}{3}P\delta_{ij}\right),\end{aligned} \tag{5}$$

where $D_f(\overline{u_i u_j})$ is the diffusion term, $P = \overline{u_i u_j}\frac{\partial \overline{U_i}}{\partial x_j}$ is the production term in the transport equation for E, and the values of the constants are suggested to be $C_1 = 1.5$ and $C_2 = 0.4$.

In order to convert the differential equation (5) to an algebraic relation, Pope adopted an approximation proposed by Rodi (1972). Rodi assumed that the transport of $\overline{u_i u_j}$, including the rate of change, advection and diffusion terms, is proportional to the transport of the kinetic energy E with the proportionality factor being the ratio $\overline{u_i u_j}/E$ (which is not a constant). One writes

$$\frac{d\overline{u_i u_j}}{dt} - D_f(\overline{u_i u_j}) = \frac{\overline{u_i u_j}}{E}\left(\frac{dE}{dt} - D_f(E)\right). \tag{6}$$

On the basic of the transport equation of E

$$\frac{dE}{dt} - D_f(E) = P - \epsilon, \tag{7}$$

Equation(6) then becomes

$$\frac{d\overline{u_i u_j}}{dt} - D_f(\overline{u_i u_j}) = \frac{\overline{u_i u_j}}{E}(P - \epsilon). \tag{8}$$

Substituting Equation (8) into Equation (5) gives

$$\begin{aligned}\frac{\overline{u_i u_j}}{E}(P-\epsilon) = & -\overline{u_i u_k}\frac{\partial \overline{U_j}}{\partial x_k} - \overline{u_j u_k}\frac{\partial \overline{U_i}}{\partial x_k} - \frac{2}{3}\epsilon\delta_{ij} \\ & -C_1\frac{\epsilon}{E}\left(\overline{u_i u_j} - \frac{2}{3}\delta_{ij}E\right) + \frac{C_2+8}{11} \\ & \times\left(\overline{u_i u_k}\frac{\partial \overline{U_j}}{\partial x_k} + \overline{u_j u_k}\frac{\partial \overline{U_i}}{\partial x_k} + \frac{2}{3}P\delta_{ij}\right) \\ & -\frac{30C_2-2}{55}E\left(\frac{\partial \overline{U_i}}{\partial x_j} + \frac{\partial \overline{U_j}}{\partial x_i}\right) + \frac{8C_2-2}{11} \\ & \times\left(\overline{u_i u_k}\frac{\partial \overline{U_k}}{\partial x_j} + \overline{u_j u_k}\frac{\partial \overline{U_k}}{\partial x_i} + \frac{2}{3}P\delta_{ij}\right).\end{aligned} \tag{9}$$

Equation (9) is a set of simultaneous algebraic equations for $\overline{u_i u_j}$. Pope, using a symbolic matrix inversion, succeeded in presenting an explicit expression for $\overline{u_i u_j}$ in terms of the mean-rate of strain tensor S and the mean-vorticity tensor W defined by

$$S_{ij} = \frac{1}{2}\frac{E}{\epsilon}\left(\frac{\partial \overline{U_i}}{\partial x_j} + \frac{\partial \overline{U_j}}{\partial x_i}\right), \tag{10a}$$

$$W_{ij} = \frac{1}{2}\frac{E}{\epsilon}\left(\frac{\partial \overline{U_i}}{\partial x_j} - \frac{\partial \overline{U_j}}{\partial x_i}\right). \tag{10b}$$

In addition, Pope introduced the following abbreviated notations

$$\mathbf{SW} = S_{ik}W_{kj}, \quad \mathbf{WS} = W_{ik}S_{kj}, \quad \{\mathbf{S}^2\} = S_{ik}S_{ki}, \quad \{\mathbf{W}^2\} = W_{ik}W_{ki}, \tag{11a}$$

$$\mathbf{I}_3 = \begin{cases} 1, & i = j, \\ 0, & i \neq j, \end{cases} \qquad \mathbf{I}_2 = \begin{cases} 1, & i = j \neq 3, \\ 0, & i \neq j \quad \text{or} \quad i = j = 3. \end{cases} \tag{11b}$$

Pope's explicit ARSM may be expressed as

$$\mathbf{a} = -2G\left[\mathbf{S} + gb_3(\mathbf{SW} - \mathbf{WS}) + gb_2\{\mathbf{S}^2\}\left(\frac{2}{3}\mathbf{I}_3 - \mathbf{I}_2\right)\right], \tag{12}$$

with

$$a_{ij} = \frac{\overline{u_i u_j}}{E} - \frac{2}{3}\delta_{ij}, \quad \text{and} \quad G = \frac{\frac{1}{2}b_1 g}{1 - 2b_3^2 g^2\{\mathbf{W}^2\} - \frac{2}{3}b_2^2 g^2\{\mathbf{S}^2\}}, \tag{13}$$

where

$$g = \frac{1}{C_1 + \frac{P}{\epsilon} - 1}, \quad b_1 = \frac{8}{15}, \quad b_2 = \frac{5 - 9C_2}{11}, \quad b_3 = \frac{7C_2 + 1}{11}. \tag{14}$$

In Pope's formulation, as well as in some other presentations of explicit ARSMs (Taulbee, 1992; Gatski and Speziale, 1993), the ratio of the energy production and dissipation rates P/ϵ remained implicit in order to retain the linearity of the equations for the Reynolds stresses. However, in the approximations proposed by Rodi (1972) and subsequently adopted by the above authors to derive the ARSM, the constancy of P/ϵ is not assumed. Moreover, since $P/\epsilon = -a_{ij}S_{ij}$, P/ϵ should not be treated as independent of a_{ij}. In order to include the dependence of P/ϵ on a_{ij}, we have re-formulated Pope's equation for a_{ij} as follows: If we take the scalar product of both sides of Equation (12) with the strain-rate tensor S, the left hand side of Equation (12) leads to

$$\{\mathbf{aS}\} = a_{ij}S_{ij} = -\frac{P}{\epsilon}, \tag{15}$$

and the right hand side of Equation (12) leads to

$$\{-2G[\mathbf{S} + gb_3(\mathbf{SW} - \mathbf{WS}) + gb_2\{\mathbf{S}^2\}(\frac{2}{3}\mathbf{I}_3 - \mathbf{I}_2)]\mathbf{S}\}$$

$$= -2GS_{ij}S_{ij} = -2G\{\mathbf{S}^2\}. \tag{16}$$

Thus,

$$\frac{P}{\epsilon} = 2G\{\mathbf{S}^2\}, \tag{17}$$

i.e., the rate P/ϵ is expressed in terms of the strain tensor $\mathbf{S}$ and the function G. On the other hand, G is defined by Equation (13), which amounts to an additional independent relation between G and the ratio P/ϵ. From Equations (17) and (13), it is possible to eliminate P/ϵ and express G solely in terms of the gradients of the mean velocity field. As it turns out, G is the solution of the following cubic equation:

$$G^3 + \frac{C_1 - 1}{\{\mathbf{S}^2\}}G^2 + \frac{(C_1 - 1)^2 - 2b_3^2\{\mathbf{W}^2\} - (b_1 + \frac{2}{3}b_2^2)\{\mathbf{S}^2\}}{4\{\mathbf{S}^2\}^2}G$$

$$-\frac{b_1(C_1 - 1)}{8\{\mathbf{S}^2\}^2} = 0. \tag{18}$$

In this way, we have succeeded in formulating a completely explicit ARSM, where the ratio P/ϵ is no longer implicit. The detailed procedure of solving the cubic equation (18) is given in the Appendix.

The singularities observed by Gatski and Speziale (1993) in the ARSMs, where the ratio P/ϵ was implicit, no longer exist. Consequently, the regularization suggested by Gatski and Speziale is no longer needed. According to Gatski and Speziale, when the strain rates $\{\mathbf{S}^2\}$ are large, the denominator in the expression (13) for G may become zero or even negative in which case the ARSM is ill-behaved. In contrast, in our model P/ϵ is expressed explicitly in terms of the strain rates as $P/\epsilon = 2G\{\mathbf{S}^2\}$ and the coefficient g becomes inversely proportional to $\{\mathbf{S}^2\}$ according to Equation (14). Then, in Equation (13), the factor g^2 in the $\{\mathbf{S}^2\}$ term effectively prevents this term from becoming too large, therefore eliminating the singularities.

2.3. Transport Equations for E and ϵ

In Pope's formulation, the turbulent kinetic energy E and the dissipation rate ϵ are assumed to be given. In practice, Pope's model must be solved in conjunction with the transport equations for E and ϵ. The transport equations for E and ϵ solved in this study are the same as those in the standard $E - \epsilon$ model:

$$\frac{dE}{dt} = \frac{\partial}{\partial x_j}\left(\frac{\nu_t}{\sigma_\epsilon}\frac{\partial E}{\partial x_j}\right) + P - \epsilon, \tag{19}$$

$$\frac{d\epsilon}{dt} = \frac{\partial}{\partial x_j}\left(\frac{\nu_t}{\sigma_\epsilon}\frac{\partial \epsilon}{\partial x_j}\right) + \frac{\epsilon}{E}(c_{1\epsilon}P - c_{2\epsilon}\epsilon), \tag{20}$$

where σ_ϵ, σ_ϵ, $c_{1\epsilon}$ and $c_{2\epsilon}$ are model constants. In these equations, the diffusion terms of E and ϵ are modeled with a down-gradient assumption, where the eddy viscosity ν_t is given by

$$\nu_t = c_\mu \frac{E^2}{\epsilon}. \tag{21}$$

The lower boundary conditions for E and ϵ are applied at some height z_p within the surface layer

$$E(z_p) = \frac{u_*^2}{c_\mu^{1/2}}, \tag{22}$$

$$\epsilon(z_p) = \frac{u_*^3}{\kappa z_p}. \tag{23}$$

The friction velocity u_* is obtained from the logarithmic profile of the mean velocity $\overline{U}$ at z_p,

$$\overline{U}(z_p) = \frac{u_*}{\kappa} ln\left(\frac{z_p}{z_0}\right), \tag{24}$$

where z_0 is the roughness length and κ is the von Karman constant.

The numerical method of obtaining the solutions of the E and ϵ equations can be found in Ying *et al.* (1994).

2.4. The transport equation for $\overline{uw}$

In the first part of this study, we use Pope's formulation to calculate all the components in the Reynolds stress tensor, while in the second part, we use Pope's formulation only to calculate the normal stresses and leave the shear stress $\overline{uw}$ to be determined by a transport equation. The transport equation for $\overline{uw}$ is

$$\frac{d\overline{uw}}{dt} = \frac{\partial}{\partial z}\left(\alpha^2 \frac{E^2}{\epsilon} \frac{\partial \overline{uw}}{\partial z}\right) + c_\phi \left[\frac{\epsilon}{E}\overline{uw} + \alpha^2 E\left(\frac{\partial \overline{U}}{\partial z} + \frac{\partial \overline{W}}{\partial x}\right)\right], \tag{25}$$

where the constants $\alpha^2 = 0.0256$ and $c_\phi = 1.5$. Equation (25) is similar to the one derived by Hanjalic and Launder (1972).

The lower boundary condition for $\overline{uw}$ is applied at $z = 0$

$$\overline{uw}(z = 0) = -u_*^2. \tag{26}$$

The numerical method of obtaining the solution for Equation (25) is given in Ying *et al.* (1994).

3. The EPA Wind Tunnel Experiment RUSHIL

The EPA wind-tunnel experiment RUSHIL (Khurshudyan *et al.*, 1981) simulates a neutral atmospheric boundary layer with two-dimensional relief. The incoming flow (in the x direction) is characterized by a logarithmic velocity profile

$$\overline{U}(z) = \frac{u_*}{\kappa} \ln\left(\frac{z}{z_0}\right), \tag{27}$$

with $z_0 = 0.157 \times 10^{-3}$ m, $u_* = 0.178$ m s^{-1}, and $\kappa = 0.4$. This velocity profile reaches the free-stream velocity $U_\infty = 3.9$ m s^{-1} at the height of 1 m. A two-dimensional model hill of analytical shape is placed across the incoming flow, spanning the width of the tunnel (in the y direction). The shape of the hill is given by the following parametric equations:

$$x = \frac{1}{2}\xi\left[1 + \frac{a^2}{\xi^2 + m^2(a^2 - \xi^2)}\right], \quad |x| \leq a \tag{28}$$

$$z = \frac{1}{2}m\sqrt{a^2 - \xi^2}\left[1 - \frac{a^2}{\xi^2 + m^2(a^2 - \xi^2)}\right], \tag{29}$$

where

$$m = \frac{h}{a} + \sqrt{\left(\frac{h}{a}\right) + 1}, \tag{30}$$

h is the height of the hill, a is the half width of the hill and ξ is an arbitrary parameter. Three different model hills with $h = 0.117$ m and different slope were used. Their aspect ratio a/h was 8, 5 and 3, corresponding to maximum slope angles of 10°, 16° and 26°, respectively. These aspect ratios will be used as hill identifiers: Hill 8, Hill 5 and Hill 3.

Measurements of mean and turbulent velocity fields were taken upwind, over and downwind of each of the hills. Vertical profiles of the mean horizontal velocity $\overline{U}(z)$, the angle of mean velocity to horizontal surface $\Phi(z)$, the longitudinal and vertical turbulent intensities $\sigma_u(z)$ and $\sigma_w(z)$, and the Reynolds shear stress $\overline{uw}(z)$ were measured at 16 longitudinal locations from $x/a = -2$ to $x/a \geq 5$, where $x = 0$ corresponds to the top of the hill. For reference purpose, all the measurements were also taken over the flat wind tunnel floor.

4. Simulations of the Mean and Turbulent Velocity Fields over Flat Terrain

In order to adjust the model parameters appearing in the turbulence models, we begin the simulation for the case of flat terrain. The standard values of these

parameters used in most applications were based on extensive examination of engineering flows (Launder and Spalding, 1974). When these models are applied to the atmospheric boundary layer, the values of these constants often need to be re-adjusted (Detering and Etling, 1985; Duynkerke, 1988). Using the data measured over a flat floor in the experiment RUSHIL, we are able to do the re-adjustment suited to a wind-tunnel experiment which simulates the atmospheric boundary layer.

First, the constant c_μ, which, from the boundary condition for Equation (22), relates the value of E in the surface layer to the friction velocity u_*, should be determined from the measurement. In the RUSHIL experiment, near the surface, the measured values of the turbulence intensities, $\sigma_u \sim 2.5u_*$, $\sigma_v \sim 1.8u_*$, $\sigma_w \sim 1.4u_*$, are in good agreement with other investigations of simulated and atmospheric boundary layers (Hunt and Fernholz, 1975; Counhan, 1975). Therefore, we use $c_\mu = 0.0256$ taken from atmospheric surface-layer observations (Panofsky *et al.*, 1977).

Next, since it is well known in the standard E–ϵ model, the constants in the ϵ equation satisfy the following relation

$$c_{1\epsilon} - c_{2\epsilon} = \frac{\kappa^2}{\sigma_\epsilon c_\mu^{1/2}}, \tag{31}$$

the adjustment of the value of c_μ inevitably affects the other constants. Using the standard E–ϵ model, we calculated the mean velocity $\overline{U}$ and the shear stress $\overline{uw}$ in the RUSHIL experiment over flat terrain. Our experimentation with varying constants leads to the same conclusion as the one reached by Detering and Etling (1985) in an earlier study: as long as relation (31) holds, the results for $\overline{U}$ and $\overline{uw}$ are only slightly dependent on the value of c_μ. However, if all the constants are kept fixed except $c_{1\epsilon}$ and $c_{2\epsilon}$, the results for $\overline{U}$ and $\overline{uw}$ are very sensitive with respect to the variation of either $c_{1\epsilon}$ or $c_{2\epsilon}$. Since $c_{2\epsilon}$ is the only constant that can be determined by experiments (Rodi, 1984), we use the widely accepted value $c_{2\epsilon} = 1.92$ and vary $c_{1\epsilon}$ in such a way that the resulting simulation profiles for $\overline{U}$ and $\overline{uw}$ agree well with the measurements. The value of $c_{1\epsilon}$ thus determined is 0.94.

Then, Pope's formulation was used to calculate the Reynolds stresses. In flat terrain, the expression for $\overline{uw}$ reduces to

$$\overline{uw} = -G\frac{E^2}{\epsilon}\frac{\partial \overline{U}}{\partial z}, \tag{32}$$

with G given by Equation (18). Comparing with the standard E–ϵ model, which gives

$$\overline{uw} = -c_\mu\frac{E^2}{\epsilon}\frac{\partial \overline{U}}{\partial z}, \tag{33}$$

over flat terrain, the coefficient G in Equation (32) should play more or less the same role as c_μ in Equation (33). Therefore, the value of G given by Equation (18) (which is not a constant) is required to be in the vicinity of 0.0256 for this study. We find that to fulfil this requirement, constant b_1 should equal 0.233 instead of 8/15 given by Pope in (14). Thus, all the constants in the turbulence model are specified.

The vertical profiles obtained from the simulations of the mean velocity $\overline{U}$, the shear stress $\overline{uw}$, and the turbulence intensities σ_u and σ_w over a flat floor, by using Pope's formulation, are given in Figure 1. In this paper, we present all the figures in a dimensionless form: the mean velocities $\overline{U}$ and $\overline{W}$ and the turbulent intensities σ_u and σ_w are normalized by the upstream friction velocity u_* given in Equation (27); the shear stress $\overline{uw}$ by u_*^2 and the height by the roughness length z_0 also given in Equation (27). Figure 1 shows good agreement between the simulation results and measurements except for some differences observed near the surface. Most remarkable are the results for σ_u and σ_w. For comparison purposes, in Figures 1c and 1d we also plot the results given by the eddy viscosity assumption, $\sigma_u = \sigma_w = \sqrt{2E/3}$ with E given by the simulation results. It is clear that Pope's formulation successfully predicts the difference between the normal stresses, and is therefore superior to models based on the eddy-viscosity assumption (1).

5. Simulations of Turbulent Flow over Hills

The vertical profiles of the horizontal wind component $\overline{U}(z)$, the vertical wind component $\overline{W}(z)$, the turbulence intensities $\sigma_u(z)$ and $\sigma_w(z)$, and the Reynolds shear stress $\overline{uw}(z)$ computed for Hills 8, 5 and 3 using Pope's formulation are compared with all available experimental profiles at 16 longitudinal locations.

As mentioned in the Introduction, the flow over hills can be divided into inner and outer layers. The justification of this division is the essentially different dynamical processes that dominate in each region. In brief, there are two fundamental time scales: the first one is the "time of flight" T_a, which is the travel time for an eddy starting upstream to be advected along a streamline; the second is the turbulent time scale T_t, which is the time taken for an eddy to decay or turnover. The changes in the structure of turbulence over a hill depend on the relative magnitude of these two scales. In the outer region, defined by $T_a < T_t$, the upstream boundary-layer turbulence is subject to rapid distortion. In the rapid distortion theory, it is assumed that the turbulence eddies are distorted by the mean flow so rapidly that the turbulence is not significantly modified by the change of strain rate (i.e., by the production term). Consequently, in the outer region, the change in turbulence depends on the history of the mean flow and not on the local velocity gradient. In a thin inner layer adjacent to the surface, defined by $T_a > T_t$, eddies encounter little change in the strain through their life time, so that the turbulence can reach an equilibrium with the perturbed mean flow. In this region, the turbulent production and dissipation

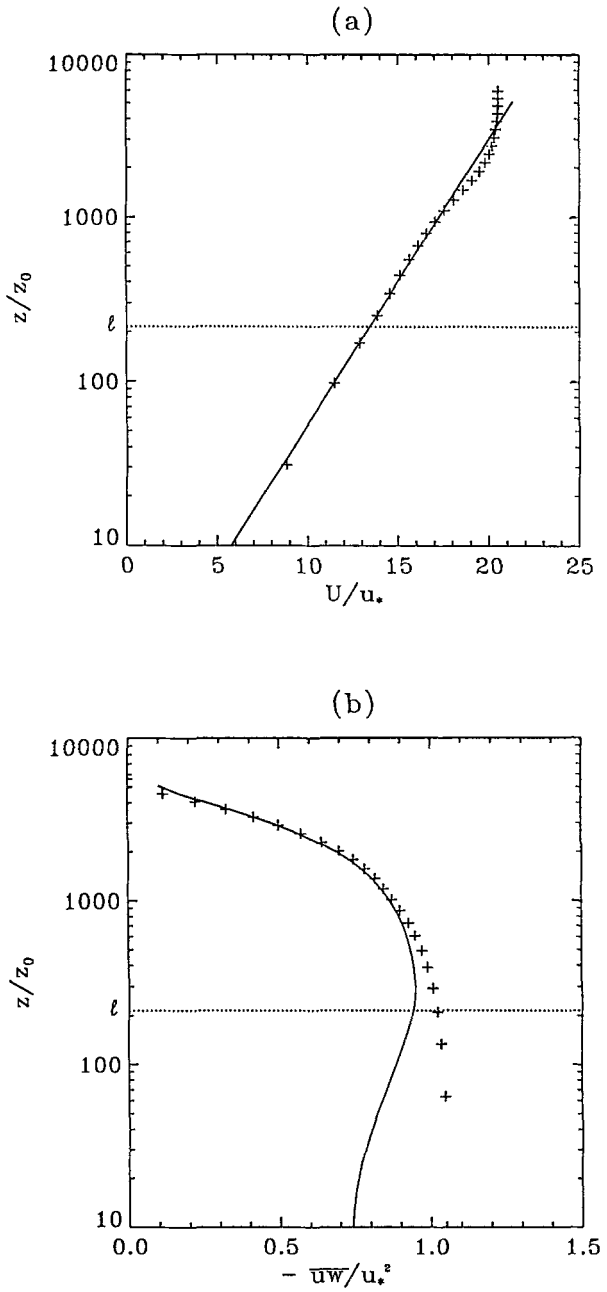

Fig. 1a–b. The vertical profiles of (a) the horizontal mean velocity $\overline{U}(z)$, (b) the Reynolds shear stress $\overline{uw}(z)$, (c) the longitudinal turbulence intensity $\sigma_u(z)$, and (d) the vertical turbulence intensity $\sigma_w(z)$ over flat terrain. The solid line is from the experimental data; the plus signs are the simulation results with Pope's model; the diamonds are the results from the eddy-viscosity approximation, where $\sigma_u(z) = \sigma_w(z) = 2E(z)/3$ with $E(z)$ given by simulations.

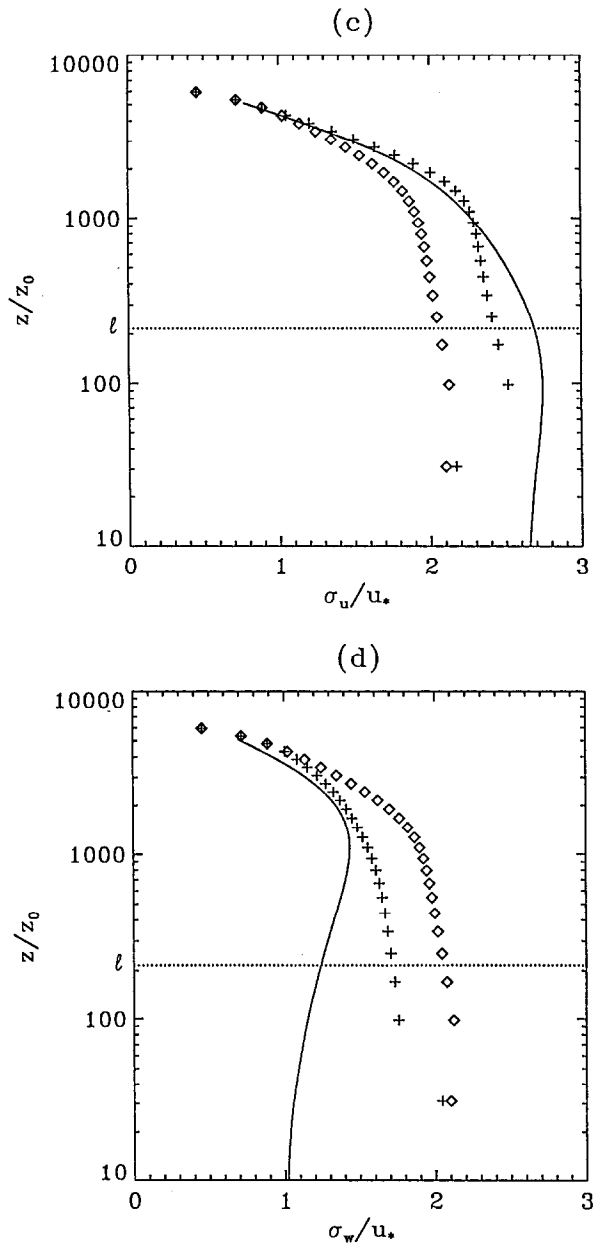

Fig. 1c–d.

dominate, and the condition for a local equilibrium is satisfied. In the intermediate region, where $T_a \sim T_t$, it is clear that the changes in the turbulence are diverse, i.e., the production, diffusion, advection, dissipation and the nonlinear process of

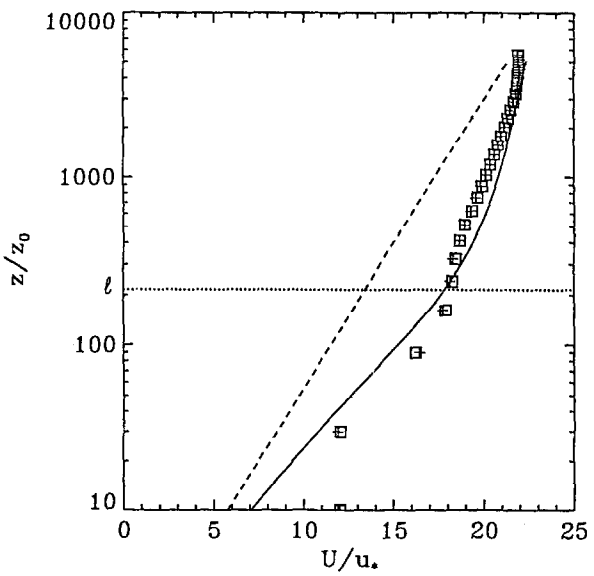

Fig. 2. The vertical profiles of the horizontal mean velocity $\overline{U}(z)$ at the top of Hill 8. The solid line is from the experimental data for Hill 8; the dashed line is from the experimental data for flat terrain; the squares are the simulation results with Pope's model; the plus signs are the simulation results with the Pope-$\overline{uw}$ model.

pressure correlation are all of comparable importance. Therefore, the turbulence changes cannot be described by either rapid distortion or local equilibrium.

Based on this analysis, the height of the inner layer ℓ is defined as the height above the hill at which the turbulence time scale $T_t(\sim E/\epsilon)$ is roughly equal to the time of flight $T_a(\sim L/\overline{U})$, where L is the distance from the crest of the hill to the half-height position of the hill. Jackson and Hunt (1975) gave the following expression to determine ℓ

$$\frac{\ell}{L}\ln\left(\frac{\ell}{z_0}\right) = 2\kappa^2. \tag{34}$$

In presenting the results for flow over a hill, we labeled the inner layer height ℓ in all the graphs.

The simulation results for the mean velocity profiles $\overline{U}(z)$ and $\overline{W}(z)$ all agree well with the wind-tunnel data and are insensitive to the particular closure scheme chosen. Since these results are similar to those presented in our previous study (Ying *et al.*, 1994), here we only present the profile of $\overline{U}$ at the top of Hill 8 in Figure 2.

When presenting the simulation results for the Reynolds stresses, we need to point out that all the measurements over hills were made with hot-wire anemometers (HWA) (Khurshudyan *et al.*, 1981). According to a report on another wind-tunnel experiment RUSVIL (Snyder *et al.*, 1991), the HWA is a convenient instrument to

use where the turbulence intensities are relatively low and the flow is not reversing. Since in the lee of Hill 5 and Hill 3, the flows are highly turbulent and reversing, the measured data are likely to be erroneous. In this paper, to avoid the confusion caused by the doubtful measurements and to concentrate on analyzing the model results, we present only the results of Reynolds stresses for Hill 8.

In Figure 3, the vertical profiles of the longitudinal turbulence intensity σ_u at three representative longitudinal locations (upstream, at hill top and downstream) obtained from the simulations with Hill 8 by using Pope's formulation are compared with the corresponding measurements. Overall, the simulation results agree well with the measurements except in the inner layer where the predicted σ_u is somewhat smaller than the measured one.

In Figure 4, the modeled vertical profiles of the vertical turbulence intensity σ_w at three representative longitudinal locations are compared with the corresponding measurements. The simulation results for σ_w are acceptable. The disagreement between the simulation results and the measurements mainly occurs in the inner layer (a feature that is exaggerated by the logarithmic height scale), where the simulation results don't quite follow the experimental trend of decreasing σ_w. We notice that this experimental trend appears consistently throughout all the measurements including those over the flat floor. There are hardly any other complete wind-tunnel measurements of σ_w that we can use to make quantitative comparison with the RUSHIL data, though some qualitative comparison is possible. For example, we can refer to the wind-tunnel study by Finnigan *et al.* (1990), in which the vertical profiles of the measured $\overline{w^2}$ are given at different longitudinal locations for flow over a hill with an aspect ratio of 6. Similar trends of decreasing $\overline{w^2}$ in the inner layer are shown at all locations. At any rate, the RUSHIL measurements seem to show a general trend of $\overline{w^2}$ near the ground, so the description of σ_w by Pope's formulation needs further improvement in the inner layer.

We believe that the disagreement between the simulation results and the measurements in the inner layer is mainly attributed to the neglect of the wall-correction term in the Reynolds stress equations. It is known that in formulating Launder *et al.*'s expression for the pressure correlation, a surface integral term, which corresponds to the pressure reflection from the wall, was neglected. Although this term does not contribute in a free shear flow, it does have a significant effect in the near-wall region. To take into account this wall-reflection effect, several researchers proposed near-wall correction terms to be added to the pressure correlation in the presence of a wall. However, adding any wall-correction term to the ARSM will inevitably destroy the linearity of the equation, thus rendering the derivation of an explicit expression for the Reynolds stress impossible. Therefore, we are forced to exclude the wall-correction term. A summary of experimental data (Launder *et al.*, 1975) shows that near a wall $\overline{u^2}$ is appreciably larger and $\overline{w^2}$ is much smaller than in the homogeneous free shear flow. The magnitude of $\overline{uw}$ is also appreciably smaller in the near-wall region. Consequently, the wall effect increases the anisotropy

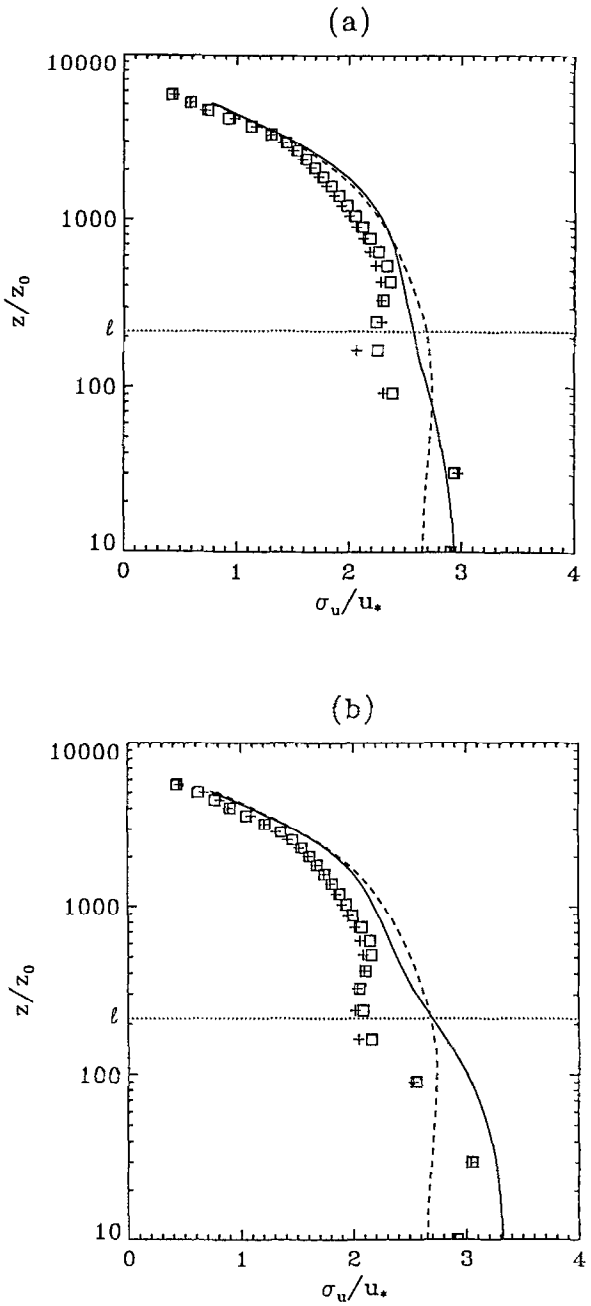

Fig. 3a–b. The vertical profiles of the longitudinal turbulence intensity $\sigma_u(z)$ over Hill 8 at three longitudinal locations: (a) $x = -a/2$, (b) $x = 0$, (c) $x = 3a/4$. The solid line is from the experimental data for Hill 8; the dashed line is from the experimental data for flat terrain; the squares are the simulation results with Pope's model; the plus signs are the simulation results with the Pope-$\overline{uw}$ model.

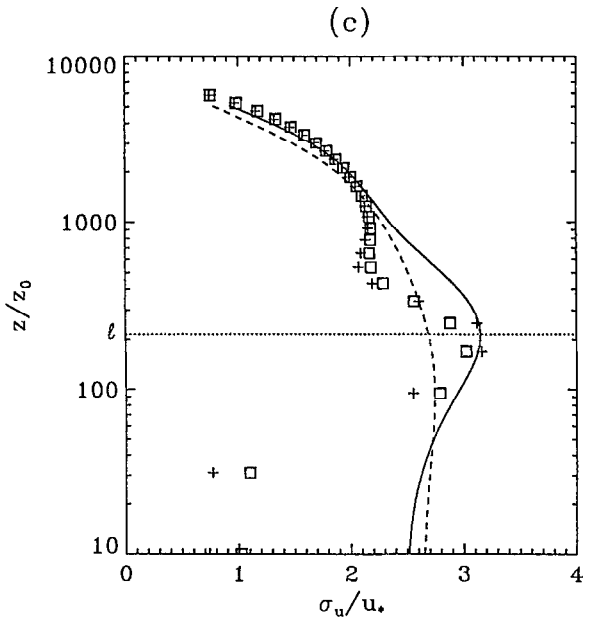

Fig. 3c.

of the normal stresses but tends to diminish the shear stress. The addition of the wall-correction term would bring about exactly this effect.

From Figures 1, 3 and 4, in both flat floor and Hill 8 cases, our simulated results for $\overline{u^2}$ in the inner layer are smaller than the measured data, and the results for $\overline{w^2}$ are considerably larger than the measured data. If a wall-correction were added to the equation, it would generally increase $\overline{u^2}$ and decrease $\overline{w^2}$ in the inner layer. Moreover, by adjusting the constants contained in the wall-correction term, it is possible to match the experimental values quite closely.

As for future improvement, we think there is a need to invent a feasible way to include the near-wall effect in the Reynolds stress equation. Since some researchers (Prud'homme, 1984; Newley, 1985) pointed out that the proposed near-wall corrections were not successful, to achieve this goal other means have been used. Launder and Li (1994) recognized that the explicit modeling of the "wall reflection" process endemically brings in undesirable parameters such as the distance from the wall. They proposed, therefore, a general cubic formulation for the pressure correlation not containing such parameters, which was well tested in many flows near walls. However, due to the non-linear nature of their formulation, it can not be incorporated into the derivation of an explicit Reynolds stress equation.

We also used Pope's formulation to calculate the shear stress $\overline{uw}$. Figure 5 shows the vertical profiles of $\overline{uw}(z)$ at three longitudinal locations of Hill 8. It is obvious that at the hill top, the predicted values of $-\overline{uw}$ are too small compared with the measurements. This disagreement may be contributed to an inadequate modeling

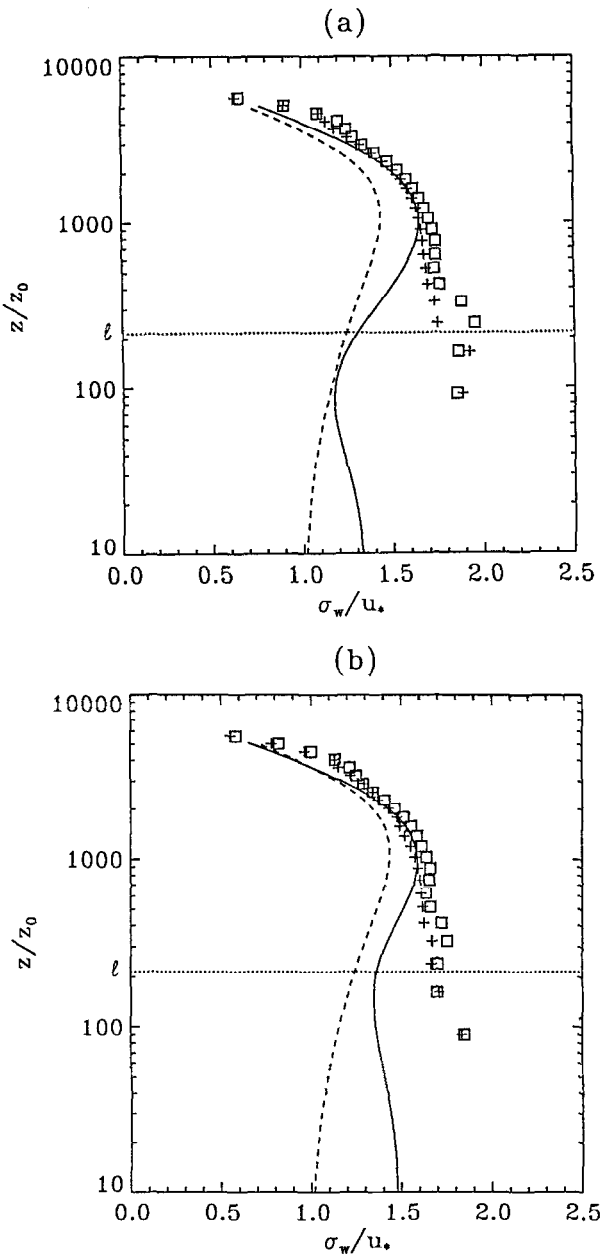

Fig. 4a–b. The same as Figure 3 but for the vertical turbulence intensity $\sigma_w(z)$.

of the turbulence transport terms in the $\overline{ww}$ equation, which involves the major approximation made in the Pope's model. Since, as analyzed before, in the outer layer the advection of upstream turbulence has a dominant effect on the turbulence characteristics, an adequate modeling of the turbulence transport term plays a vital

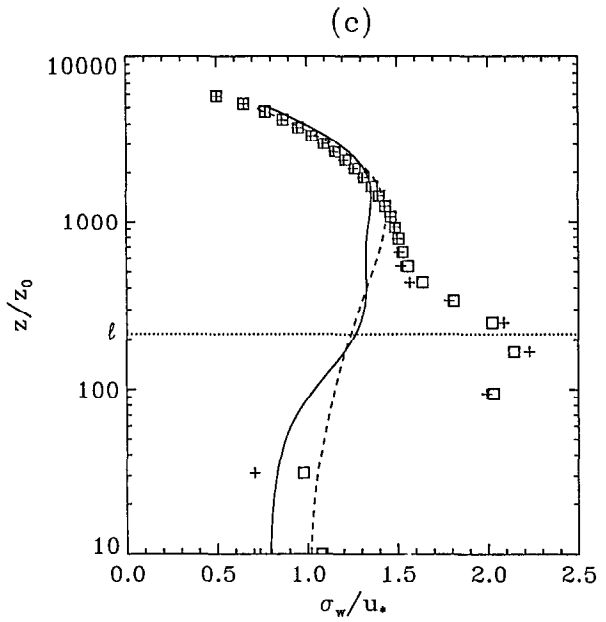

Fig. 4c.

role in the whole formulation. As far as the upstream profile of $\overline{uw}$ is concerned, the modelled results seem to agree well with the measurements except in the inner layer. For the downstream profile of $\overline{uw}$, we obtained results quite similar to those in our previous study (Ying *et al.*, 1994) and the detailed discussion there will not be repeated here. In brief, the disagreement between the modelled results and measurements is most likely due to the measurement errors caused by an improper instrument (HWA) used to measure the high intensity turbulence in the lee.

We recall that the major approximation made in the derivation of the algebraic equation for the Reynolds stress $\overline{u_i u_j}$ is assuming that the transport of $\overline{u_i u_j}$ is proportional to that of the turbulent energy E with proportionality factor being the ratio $\overline{u_i u_j}/E$. The validity of this approximation obviously depends on how closely the individual Reynolds stress component behaves like the turbulent energy E. Since half of the sum of the three normal stresses $\overline{u^2}$, $\overline{v^2}$ and $\overline{w^2}$ equals the turbulent energy E, as long as these three components themselves behave in a similar manner, the above-mentioned approximation should be valid for all the normal stresses. An inspection of the RUSHIL experimental data of σ_u and σ_w at 16 different longitudinal locations upstream of, over and downstream of the hill shows that in the outer layer there is no perceivable redistribution among the three components. The two components $\overline{u^2}$ and $\overline{w^2}$, which together account for more than 70% of the total sum, behave very much the same. These facts seem to support the validity of the approximation. As shown in Figures 3 and 4, the model results for σ_u and σ_w in the outer layer indeed agree well with the experimental data.

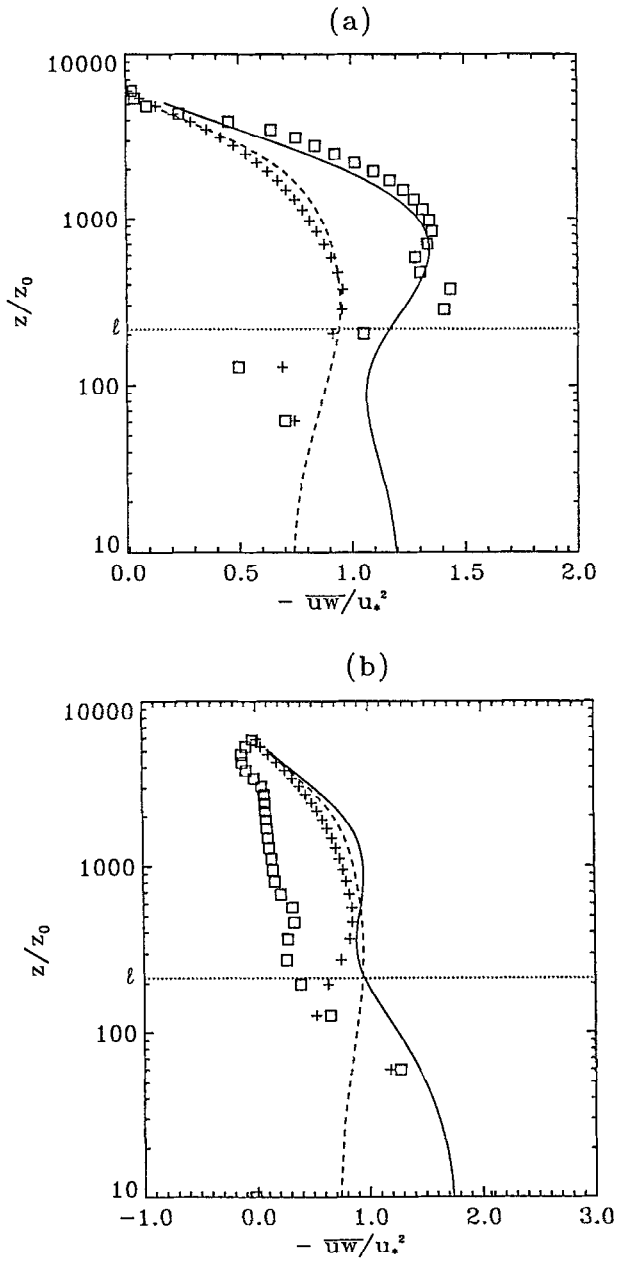

Fig. 5a–b. The same as Figure 3 but for the Reynolds shear stress $\overline{uw}(z)$.

As for the shear stress $\overline{uw}$, the assumption that it is advected and diffused in a similar manner to the turbulent energy E lacks a sound physical basis since there is no direct connection between these two quantities. In fact, by analyzing the transport equations for $\overline{uw}$ and E in the streamline coordinate system, both Zeman

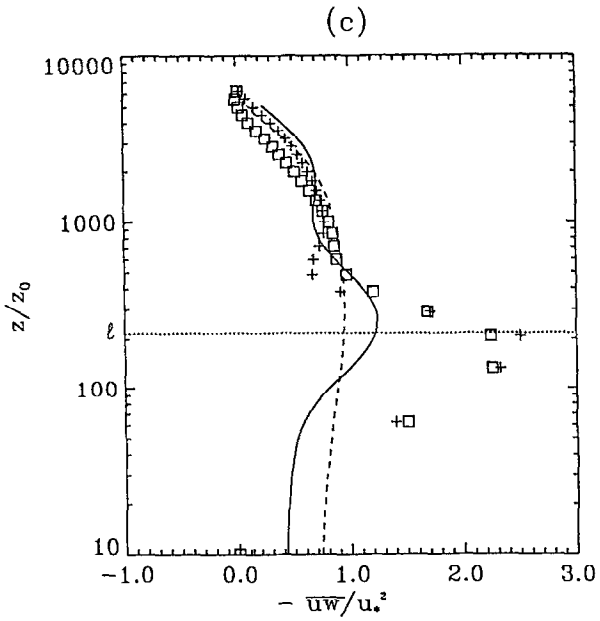

Fig. 5c.

and Jensen (1985) and Kaimal and Finnigan (1994) pointed out that in the case of flow over hills E is most sensitive to the flow acceleration and $\overline{uw}$ is dominated by the curvature of the streamline. These two distinct types of mechanism result in different behaviour between $\overline{uw}$ and E, which inevitably makes the above-mentioned approximation invalid. These arguments suggest that a transport equation is needed to describe the shear stress $\overline{uw}$ in hilly terrain.

In the second turbulence model, the Pope-$\overline{uw}$ model, we solve a transport equation for $\overline{uw}$, Equation (25), while still using Pope's formulation to calculate the normal stresses $\overline{u^2}$, $\overline{v^2}$ and $\overline{w^2}$. Figures 3 and 4 show that the results for the turbulence intensities σ_u and σ_w change very little from those calculated in the first model. On the other hand, Figure 5b shows a dramatically improved result for $\overline{uw}$ at the hill top from the new closure scheme, which indicates that a transport equation for $\overline{uw}$ can indeed adequately model the advection effect. Nevertheless, the simulations are more successful in the outer layer than in the inner layer. The analysis of the inner-layer results in our previous study of the $\overline{uw}$ transport equation (Ying *et al.*, 1994) also holds true here.

In Figures 6, 7 and 8, the streamwise profiles of σ_u, σ_w and $\overline{uw}$ are presented along three constant η lines in the terrain-following coordinate system, which are located in the inner, middle and outer layers, respectively. The reason why we choose the profiles along lines with constant η values instead of constant z values is that these lines are good approximations to the streamlines and it is much easier to discuss the behaviour of the Reynolds stresses over a hill along the streamlines.

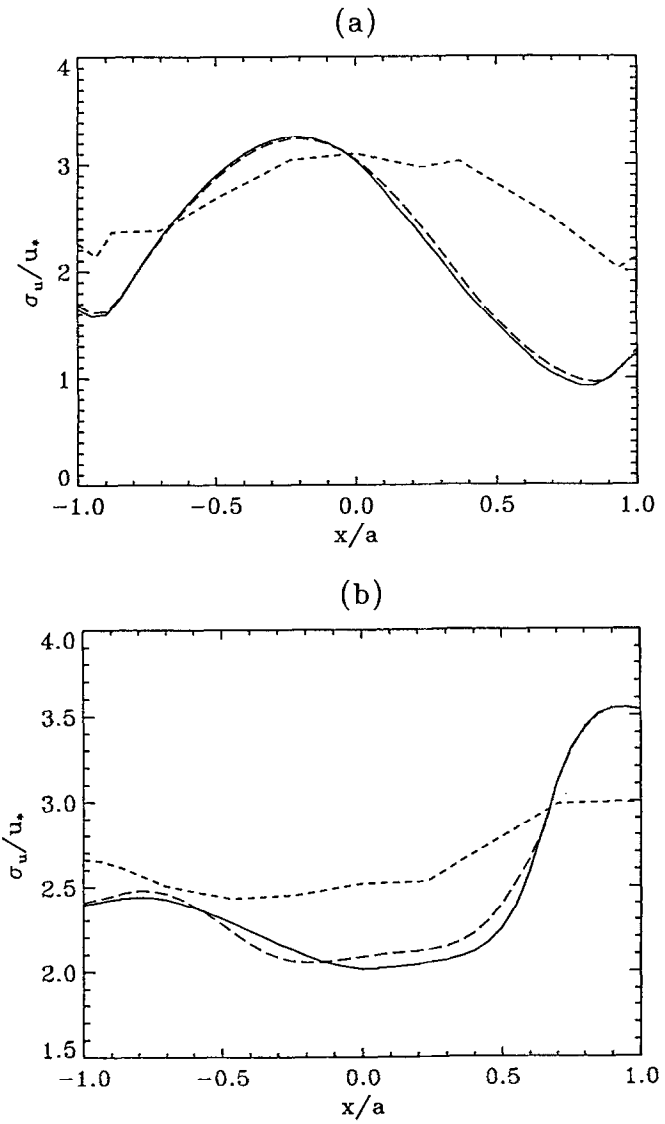

Fig. 6a–b. The streamwise profiles of the longitudinal turbulence intensity $\sigma_u(x)$ over Hill 8 along three lines with constant η values: (a) $\eta = 0.005$, (b) $\eta = 0.04$, (c) $\eta = 0.34$. The solid line is the simulation results with the Pope-$\overline{uw}$ model; the long-dashed line is the simulation results with Pope's model; the dashed line is from the experimental data.

Figures 6a and 7a show the streamwise profiles of σ_u and σ_w along a fixed $\eta = 0.005$ line, which originates from the upstream height $z = 0.005m$; and Figure 8a shows the profile of $\overline{uw}$ along the $\eta = 0$ line, which coincides with the surface. These profiles are all located at the bottom of the inner layer, where local equilibrium prevails. The simulation results of all the three quantities from both

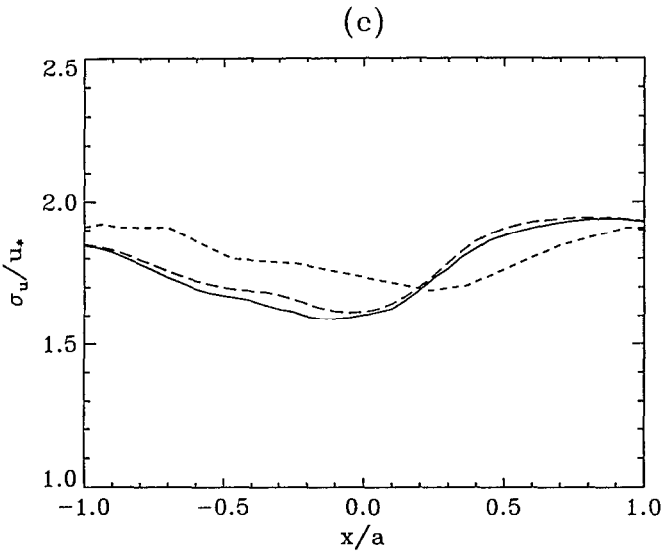

Fig. 6c.

models clearly demonstrate that at the bottom of the inner layer, the changes of the Reynolds stresses over a hill reflect the changes in the near-surface mean shear that are directly related to the upstream deceleration close to the surface, the speedup at the hill top and the deceleration in the lee. This behaviour can qualitatively be explained by the local equilibrium theory. When comparing the modelled results with the wind-tunnel measurements, we find substantial differences between them. Moreover, the measured data do not reflect the changes in the flow speed well, especially in the case of σ_w and $\overline{uw}$. It is known that the roughness elements used in the RUSHIL experiment were river-washed gravels with diameters of about 0.01 m (Khurshudyan *et al.*, 1982). Under this condition, measurements at a height of 0.005 m or less are almost impossible and the results are hardly reliable. In our opinion, for the most part one should probably disregard the experimental data in this case.

Figures 6b and 7b show the streamwise profiles of σ_u and σ_w along a fixed $\eta = 0.04$ line, which originates from the upstream height $z = 0.04m$ and is located in the middle layer. In the modelled results for σ_u, we observe a small rise in the upstream region, a decrease toward the hill top and a large increase in the lee. The modelled result of σ_w shows an increase at the upstream side of the hill, where the streamline curvature is concave, then a decrease over the hill top, where the curvature is convex, and finally an increase again in the lee.

Figures 6c and 7c show the streamwise profiles of σ_u and σ_w along a fixed $\eta = 0.34$ line, which originates from the upstream height $z = 0.34m$ and is located in the outer layer. Here, we observe that σ_u and σ_w behave in a similar

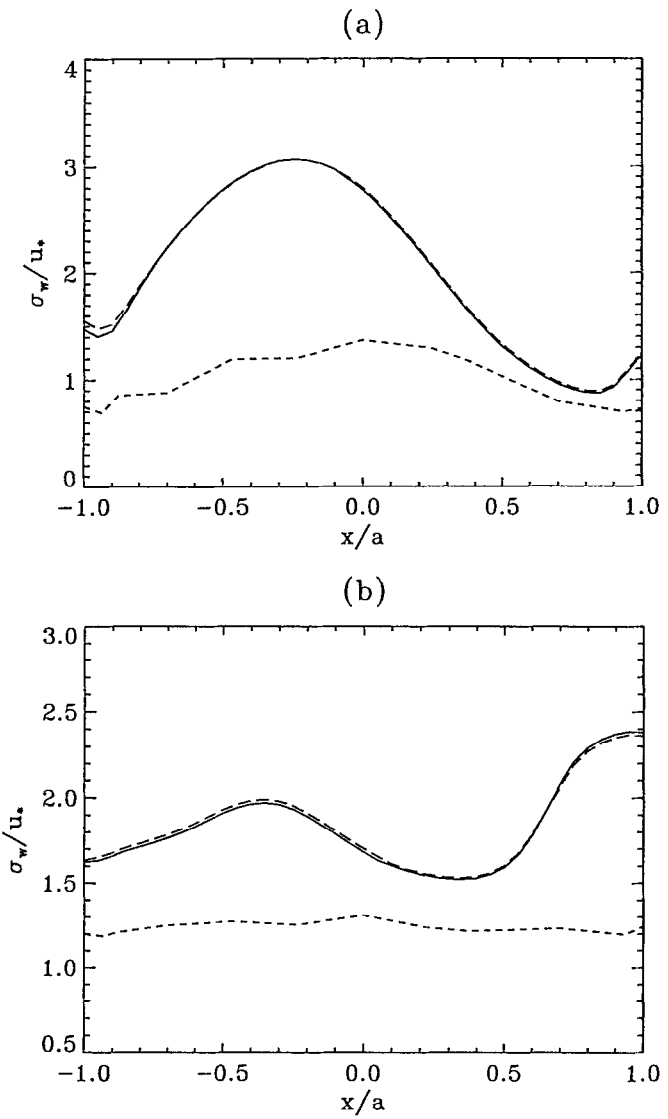

Fig. 7a–b. The same as Figure 6 but for the vertical turbulence intensity $\sigma_w(x)$.

manner as in the middle layer, with the difference that their variations over the hill are not so dramatic as in the middle layer.

In order to compare the simulation results of σ_u and σ_w in the middle and outer layers with existing theory, we need to turn to the transport equations for the Reynolds stresses written in a streamline coordinate system. Let x' and z' be the coordinates parallel and perpendicular to the flow direction, respectively, $\overline{U'}$ be the mean velocity, $\overline{u'^2}$ and $\overline{w'^2}$ be the normal stresses in the x' and z' directions,

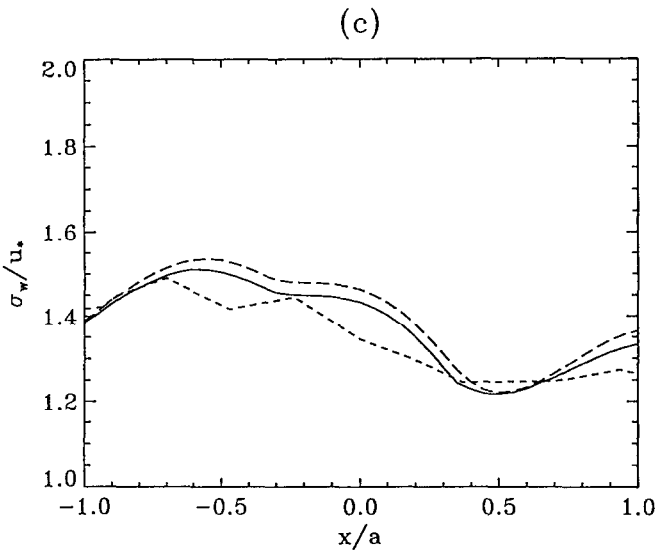

Fig. 7c.

respectively, and $\overline{u'w'}$ be the shear stress. According to Kaimal and Finnigan (1994), these equations are

$$\overline{U'}\frac{\partial \overline{u'^2}}{\partial x'} = -2\overline{u'^2}\frac{\partial \overline{U'}}{\partial x'} - 2\overline{u'w'}\frac{\partial \overline{U'}}{\partial z'} + 2\overline{u'w'}\left(\frac{\overline{U'}}{R}\right) + (\text{other terms}), \tag{35}$$

$$\overline{U'}\frac{\partial \overline{w'^2}}{\partial x'} = -4\overline{u'w'}\left(\frac{\overline{U'}}{R}\right) + 2\overline{w'^2}\frac{\partial \overline{U'}}{\partial x'} + (\text{other terms}), \tag{36}$$

$$\overline{U'}\frac{\partial \overline{u'w'}}{\partial x'} = -2\overline{u'^2}\left(\frac{\overline{U'}}{R}\right) + \overline{w'^2}\left(\frac{\overline{U'}}{R}\right) - \overline{w'^2}\frac{\partial \overline{U'}}{\partial z'} + (\text{other terms}), \tag{37}$$

where R is the radius of the streamline curvature, and (other terms) includes the diffusion, pressure-correlation and dissipation terms. It is evident that the advantage of writing the Reynolds stress equations in streamline coordinates is that the turbulence production is decoupled into individual terms, each of which can be identified with a certain physical effect, such as the streamwise flow acceleration ($\partial\overline{U'}/\partial x'$), the shear ($\partial\overline{U'}/\partial z'$) and the streamline curvature ($1/R$). Equations (35)–(37) show that $\overline{u'^2}$ is most sensitive to the streamwise acceleration, $\overline{w'^2}$ responds to both the streamline curvature and acccleration with more weight of the curvature, and $\overline{u'w'}$ is dominated by the curvature.

Even though the σ_u, σ_w and $\overline{uw}$ in our calculations are not identical to $(\overline{u'^2})^{1/2}$, $(\overline{w'^2})^{1/2}$ and $\overline{u'w'}$ in the Hill 8 case, the differences should be small at distances well away from the surface. Thus, qualitatively, the conclusions drawn for $\overline{u'^2}$, $\overline{w'^2}$ and

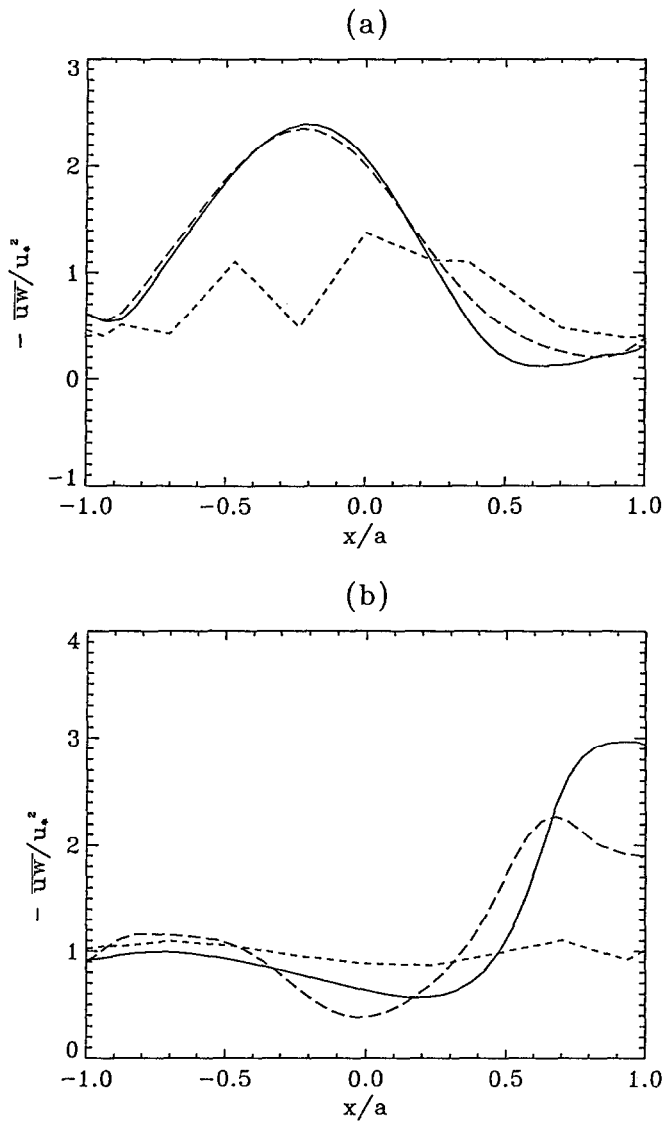

Fig. 8a–b. The streamwise profiles of the Reynolds shear stress $\overline{uw}(x)$ over Hill 8 along three lines with constant η values: (a) $\eta = 0$, (b) $\eta = 0.033$, (c) $\eta = 0.32$. The solid line is the simulation results with the Pope-$\overline{uw}$ model; the long-dashed line is the simulation results with Pope's model; the dashed line is from the experimental data.

$\overline{u'w'}$ should also apply to σ_u, σ_w and $\overline{uw}$. The variation of the modelled σ_u can very well be explained by the upstream flow deceleration, the flow acceleration toward the hill top and the flow deceleration in the lee. Moreover, it is obvious that these changes in the flow velocity are less pronounced farther away from the surface, which explains the difference between the modelled results in the outer and middle

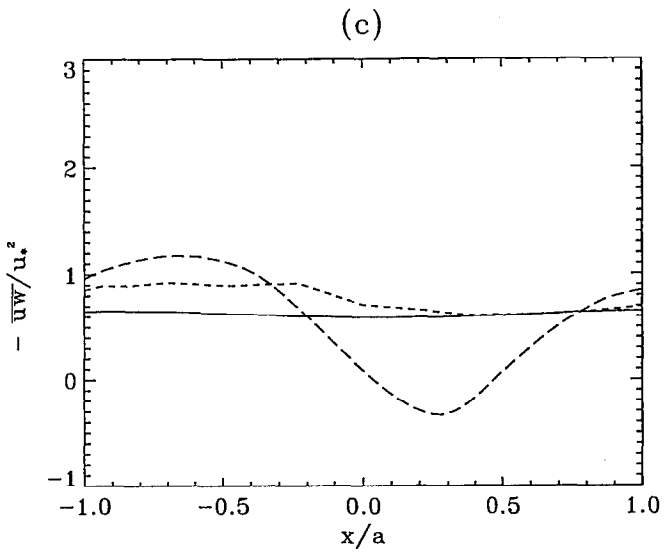

Fig. 8c.

layers. On the other hand, the behaviour of the modelled σ_w can be explained by both the curvature and acceleration effects, especially by the curvature.

From Figures 6a, 7a, 6b and 7b, we also observe that the modelled results of σ_u and σ_w in the middle and outer layers are generally close to the wind-tunnel measurements, especially in the outer layer. Nevertheless, the measured data appear to show smaller variations than the modelled results.

Figure 8b shows the modelled results of $\overline{uw}$ in the middle layer along a fixed $\eta = 0.033$ line, which originates from the upstream height $z = 0.033m$. Figure 8c shows the results of $\overline{uw}$ in the outer layer along the $\eta = 0.32$ line ($z = 0.32m$). We find the results of $\overline{uw}$ in the middle layer from both models somewhat similar to those of σ_u in the middle layer; whereas in the outer layer, the result of $\overline{uw}$ from Pope's model is similar to that of σ_w in the outer layer and the result from the Pope-$\overline{uw}$ model shows almost a constant value for $\overline{uw}$. These results don't agree with the prediction given by Equation (37) that $\overline{uw}$ should be most sensitive to the streamline curvature. We have already indicated the problem with Pope's model when used to predict $\overline{uw}$ over a hill. Now, it seems that although the Pope-$\overline{uw}$ model can describe the behavior of $\overline{uw}$ at the hill top reasonably well, it needs further improvement to correctly predict the changes of $\overline{uw}$ as flow moves over the hill. As shown in Equation (25), the transport equation for $\overline{uw}$ used in this study is indeed over-simplified, especially in the production term. Therefore, the improvement should be directed to including more physics in the transport equation, probably by using the complete form given by Equation (5). Actually, we are currently undertaking the task of implementing Equation (5) in a simulation routine.

6. Conclusions

We have performed numerical simulations of turbulent flow over two-dimensional hills with different slope using a finite-difference method in a non-hydrostatic atmospheric model. Computations of the mean flows and turbulence with two different turbulence closure schemes have been compared with measurements from the EPA wind-tunnel experiment RUSHIL. In a first model, Pope's explicit ARSM is used to calculate all the components in the Reynolds stress tensor; in a second model, Pope's formulation is combined with a transport equation for $\overline{uw}$. Our findings can be summarized as follows:

1. Previous studies on flow over complex terrain (Taylor *et al.*, 1987; Beljaars *et al.*, 1987; Ayotte *et al.*, 1994) concluded that the simulated results of the mean velocities are insensitive to the turbulence models used. In our study, the simulated mean flow results employing two different turbulence closure models all agree well with the measurements, which confirms the general assessment.

2. The simulation results for the turbulence intensities σ_u and σ_w obtained from the two turbulence models are only slightly different. The results for σ_u agree well with the measurements and the results for σ_w are acceptable but need to be improved in the inner layer. Also, the simulation results demonstrate that the changes of σ_u and σ_w as flow moves over a hill are qualitatively in agreement with those expected from existing theory.

3. Pope's formulation fails to predict the shear stress $\overline{uw}$ at hill tops. In order to adequately describe $\overline{uw}$ in hilly terrain, it is necessary to introduce a transport equation for $\overline{uw}$ in the second turbulence model. This finding coincides with the conclusions reached by a number of researchers previously (Zeman and Jensen, 1987; Beljaars *et al.*, 1987; Ayotte *et al.*, 1994). The physical reason for it has been repeatedly mentioned by these authors, that is, in the outer region, advection of upstream turbulence dominates and only a transport equation for $\overline{uw}$ can realistically model the advection effect. Although the simplified form of the transport equation used in this study is successful in predicting the behavior of $\overline{uw}$ at the hill top, it needs further improvement to correctly describe the changes of $\overline{uw}$ as flow passes over a hill.

Acknowledgement

R. Ying would like to acknowledge financial support from ENEL-CRTN. Simulations were produced with the Regional Atmospheric Modeling System (RAMS). RAMS was developed at the Colorado State University under the support of the National Science Foundation (NSF) and the Army Research Office (ARO).

Appendix: Solution of the Cubic Equation for G

Equation (18) can be written in the general form of a cubic equation

$$x^3 + ax^2 + bx + c = 0, \tag{A1}$$

where

$$a = \frac{C_1 - 1}{\{\mathbf{S}^2\}}, \tag{A2}$$

$$b = \frac{(C_1 - 1)^2 - 2b_3^2\{\mathbf{W}^2\} - (b_1 + \frac{2}{3}b_2^2)\{\mathbf{S}^2\}}{4\{\mathbf{S}^2\}^2}, \tag{A3}$$

$$c = -\frac{b_1(C_1 - 1)}{8\{\mathbf{S}^2\}^2}. \tag{A4}$$

First let

$$Q \equiv \frac{a^2 - 3b}{9} \quad \text{and} \quad R \equiv \frac{2a^3 - 9ab + 27c}{54}. \tag{A5}$$

If $R^2 - Q^3 \leq 0$, then the cubic equation has three real roots. Find them by computing

$$\theta = \arccos\left(\frac{-R}{\sqrt{Q^3}}\right), \tag{A6}$$

in terms of which, the three roots are

$$\begin{aligned} x_1 &= 2\sqrt{Q}\cos\left(\frac{\theta}{3}\right) - \frac{a}{3}, \\ x_2 &= 2\sqrt{Q}\cos\left(\frac{\theta + 2\pi}{3}\right) - \frac{a}{3}, \\ x_3 &= 2\sqrt{Q}\cos\left(\frac{\theta - 2\pi}{3}\right) - \frac{a}{3}. \end{aligned} \tag{A7}$$

If $R^2 - Q^3 > 0$, the cubic equation has only one real root. Find this root by computing

$$A = -sgn(R)\left[|R| + \sqrt{R^2 - Q^3}\right]^{1/3} \tag{A8}$$

and

$$B = \begin{cases} Q/A, & (A \neq 0), \\ 0, & (A = 0), \end{cases} \tag{A9}$$

in terms of which, the real root is

$$x = (A + B) - \frac{a}{3}. \tag{A10}$$

From the above solutions of the cubic equation, it is evident that in the case of $R^2 - Q^3 > 0$, the only real root of the equation provides a unique solution to the physical problem. However, it is not so simple in the case of $R^2 - Q^3 \leq 0$, where the physical solution must be chosen from the three real roots of the problem. Assuming $R < 0$, as $R^2 - Q^3 \to 0^-$, the unique real root x given by (A10) approaches the limit $-2R^{1/3} - a/3$; on the other hand, as $R^2 - Q^3 \to 0^+$, only root x_1 in (A7) approaches the same limit. It is obvious that when $(R^2 - Q^3)$ changes sign from positive to negative, x_1 is the only continuous solution corresponding to x. Therefore, in the case of $R^2 - Q^3 \leq 0$ and $R < 0$, we should choose x_1 as the physical solution. Actually, this is the only case that we need to discuss because from (A5) it can be easily proven that with a, b and c given by (A2), (A3) and (A4), R is always negative.

References

Ayotte, K. W., Xu, D., and Taylor, P. A.: 1994, 'The Impact of Different Turbulence Closures on Predictions of the Mixed Spectral Finite Difference Model for Flow over Topography', *Boundary-Layer Meteorol.* **68**, 1–33.

Beljaars, A. C. M., Walmsley, J. L., and Taylor, P. A.: 1987, 'A Mixed Spectral Finite-Difference Model for Neutrally Stratified Boundary-Layer Flow over Roughness Changes and Topography', *Boundary-Layer Meteorol.* **38**, 273–303.

Britter, R. E., Hunt, J. C. R., and Richard, K. J.: 1981, 'Air Flow over a Two-Dimensional Hill: Studies of Velocity Speed-up, Roughness effects and Turbulence', *Quart. J. Roy. Meteorol. Soc.* **107**, 91–110.

Clark, T. L.: 1977, 'A Small-Scale Dynamic Model Using a Terrain-Following Coordinate Transformation', *J. Computational Phys.* **24**, 186–215.

Counihan, J., 1975, 'Adiabatic Atmospheric Boundary Layers: A Review and Analysis of Data from the Period 1880-1972', *Atmos. Environ.* **9**, 871–905.

Detering, H. W. and Etling, D.: 1985, 'Application of the E–ϵ Turbulence Model to the Atmospheric Boundary Layer', *Boundary-Layer Meteorol.* **33**, 113–133.

Duynkerke, P. G.: 1988, 'Application of the E–ϵ Turbulence Closure Model to the Neutral and Stable Atmospheric Boundary Layer', *Amer. Meteorol. Soc.* **45**, 865–880.

Finnigan, J. J., Raupach, M. R., Bradley, E. F., and Aldis, G. K., 1990, 'A Wind Tunnel Study of Turbulent Flow over a Two-Dimensional Ridge', *Boundary-Layer Meteorol.* **50**, 277–317.

Gatski, T. B. and Speziale, C. G.: 1993, 'On Explicit Algebraic Stress Models for Complex Turbulent Flows', *J. Fluid Mech.* **254**, 59–78.

Hanna, S. R.: 1968, 'A Method of Estimating Vertical Eddy Transport in the Planetary Boundary Layer Using Characteristics of the Vertical Velocity Spectrum', *J. Atmos. Sci.* **25**, 1026–1033.

Hunt, J. C. R. and Fernholz, H.: 1975, 'Wind-Tunnel Simulation of the Atmospheric Boundary Layer: a Report on Euromech 50', *J. Fluid Mech.* **70**, 543–559.

Hunt, J. C. R., Leibovich, S., and Richard, K. J.: 1988, 'Turbulent Shear Flow over Low Hills', *Quart. J. Roy. Meteorol. Soc.* **114**, 1435–1470.

Jackson, P. S. and Hunt, J. C. R.: 1975, 'Turbulent Wind Flow over a Low Hill', *Quart. J. Roy. Meteorol. Soc.* **101**, 929-955.

Kaimal, J. C. and Finnigan, J. J.: 1994, *Atmospheric Boundary Layer Flows: Their Structure and Measurement*, Oxford University Press, New York.

Khurshudyan, L. H., Snyder, W. H., and Nekrasov, I. V.: 1981, 'Flow and Dispersion of Pollutants over Two-Dimensional Hills,' U.S. Envir. Prot. Agcy. Rpt. No. EPA-6000/4-81-067. *Res. Tri. Pk.*, NC., 131 pp.

Launder, B. E. and Li, S. -P.: 1994, 'On the Elimination of Wall-Topography Parameters from Second-Moment Closure', *Phys. Fluid* **6**, 999–1006.

Launder, B. E., Reece, G. J., and Rodi, W.: 1975, 'Progress in the Development of a Reynolds-Stress Turbulence Closure', *J. Fluid Mech.* **68**, 537–566.

Mason, P. J. and Sykes, R. I.: 1979, 'Flow over an Isolated Hill of Moderate Slope', *Quart. J. Roy. Meteorol. Soc.* **105**, 383–395.

Panofsky, H. A., Tennekes H., Lenschow, D. H., and Wyngaard, J. C.: 1977, 'The Characteristics of Turbulent Velocity Components in the Surface Layer under Convective Conditions', *Boundary-Layer Meteorol.* **11**, 355–361.

Pope, S. B.: 1975, 'A More General Effective-Viscosity Hypothesis', *J. Fluid Mech.* **72**, 331–340.

Rodi, W.: 1972, 'The Prediction of Free Turbulent Boundary Layers by Use of a Two-Equation model of Turbulence', Ph.D. thesis, University of London.

Rodi, W.: 1984, 'Turbulence Models and Their Application in Hydraulics', IAHR, Netherlands.

Snyder, W. H., Khurshudyan, L. H., Nekrasov, I. V., Lawson JR, R. E., and Thompson, R. S.: 1991, 'Flow and Dispersion of Pollutants within Two-Dimensional Valleys', *Atmos. Environ.* **25A**, 1347–1375.

Taulbee, D. B.: 1992, 'An Improved Algebraic Reynolds Stress Model and Corresponding Nonlinear Stress Model', *Phys. Fluids* **A 4**, 2555–2561.

Taylor, P. A., Walmsley, J. L., and Salmon, J. R.: 1983, 'A Simple Model of Neutrally Stratified Boundary-Layer Flow over Real Terrain Incorporating Wavenumber-Dependent Scaling', *Boundary-Layer Meteorol.* **26**, 169–189.

Taylor, P. A. and Teunissen, H. W.: 1985, *The Askervein Hill Project: Report on the September/October 1983 Main Field Experiment*, Internal Rep. MSRB-84-6, Atmos. Environ. Service, Downsview, Ont., Canada.

Taylor, P. A., Mason, P. I., and Bradley, E. F.: 1987, 'Boundary-Layer Flow over Low Hills', *Boundary-Layer Meteorol.* **39**, 107–132.

Walmsley, J. L., Salmon, J. R., and Taylor, P. A.: 1982, 'On the Application of a Model of Boundary-Layer Flow over Low Hills to Real Terrain', *Boundary-Layer Meteorol.* **23**, 17–46.

Walmsley, J. L., Taylor, P. A., and Keith, T.: 1986, 'A Simple Model of Neutrally Stratified Boundary-Layer Flow over Complex Terrain with Surface Roughness Modulations (MS3DJH/3R)', *Boundary- Layer Meteorol.* **36**, 157–186.

Xu, D., Ayotte, K. W. and Taylor, P. A.: 1994, 'Development of a Non-Linear Mixed Spectral Finite Difference Model for Turbulent Boundary-Layer Flow over Topography', *Boundary-Layer Meteorol.* **70**, 341–367.

Ying, R., Canuto, V. M., and Ypma, R. M.: 1994, 'Numerical Simulation of Flow Data over Two-Dimensional Hills', *Boundary-Layer Meteorol.* **70**, 401–427.

Zeman, O. and Jensen, N. O.: 1987, 'Modification of Turbulence Characteristic in Flow over Hills', *Quart. J. Roy. Meteorol. Soc.* **113**, 55–80.